MOLECULAR AND CELLULAR BIOLOGY, Feb. 2008, p. 1029–1040 Vol. 28, No. 3
0270-7306/08/$08.00+0 doi:10.1128/MCB.01247-07

Annexin A2 Phosphorylation Mediates Cell Scattering and Branching Morphogenesis via Cofilin Activation▽†

Marjo de Graauw,[1] Ine Tijdens,[1] Mirjam B. Smeets,[3] Paul J. Hensbergen,[2] André M. Deelder,[2] and Bob van de Water[1]*

Division of Toxicology, Leiden/Amsterdam Center for Drug Research, Leiden University, 2300 RA, Leiden, The Netherlands[1]; Biomolecular Mass Spectrometry Unit, Department of Parasitology, Leiden University Medical Center, 2300 RC Leiden, The Netherlands[2]; and Experimental Cardiology Laboratory, Department of Cardiology, UMC, Utrecht, The Netherlands[3]

Received 12 July 2007/Returned for modification 6 August 2007/Accepted 12 November 2007

Dynamic remodeling of the actin cytoskeleton is required for cell spreading, motility, and migration and can be regulated by tyrosine kinase activity. Phosphotyrosine proteomic screening revealed phosphorylation of the lipid-, calcium-, and actin-binding protein annexin A2 (AnxA2) at Tyr23 as a major event preceding *ts*-v-Src kinase-induced cell scattering. Expression of the phospho-mimicking mutant Y23E-AnxA2 itself was sufficient to induce actin reorganization and cell scattering in MDCK cells. While Y23E-AnxA2, but not Y23A-AnxA2, enhanced Src- or hepatocyte growth factor (HGF)-induced cell scattering, short hairpin RNA-mediated knockdown of AnxA2 inhibited both v-Src- and HGF-induced cell scattering. Three-dimensional branching morphogenesis was induced in wild-type-AnxA2-expressing cells only in the presence of HGF, while Y23E-AnxA2 induced HGF-independent branching morphogenesis. Knockdown of AnxA2 prevented lumen formation during cystogenesis. The Y23E-AnxA2-induced scattering was associated with dephosphorylation/activation of the actin-severing protein cofilin. Likewise, inactive S3E-cofilin and constitutively active LIM kinase, a direct upstream kinase of cofilin, inhibited Y23E-AnxA2-induced scattering. Together, our studies indicate an essential role for AnxA2 phosphorylation in regulating cofilin-dependent actin cytoskeletal dynamics in the context of cell scattering and branching morphogenesis.

The epithelial mesenchymal transition (EMT) is a highly conserved and important process regulating morphogenesis, tissue restructuring, and tumor progression in multicellular organisms (33, 36). The transition process is characterized by loss of cell-cell interaction in association with an active, well-controlled rearrangement of the F-actin cytoskeletal network. In time, epithelial cells acquire a scattered and highly motile phenotype, allowing migration away from an established, tightly adherent cellular environment.

The onset of epithelial cell scattering is, among other events, controlled by receptor tyrosine kinases, such as the hepatocyte growth factor (HGF) receptor c-Met (36). In addition to cell scattering, HGF induces branching morphogenesis of cells when they are cultured in three-dimensional (3D) collagen (Cn) gels (21). HGF-triggered signaling downstream of c-Met is mediated by nonreceptor tyrosine kinases, including Src kinase family members (23). Activated Src kinase causes tyrosine phosphorylation (pTyr) of various cellular proteins, including cytoskeletal and cell adhesion proteins that can influence the adhesive phenotype of epithelial cells (3, 15, 27). Most likely, these Src-phosphorylated adhesion- and/or cytoskeleton-regulating proteins mediate the onset of cell scattering, followed by EMT. Therefore, a phosphotyrosine (PY) proteome-wide characterization of Src kinase substrates and candidate EMT regulating proteins is required.

To identify Src substrates that may mediate cell scattering, we used conditional v-Src kinase-induced scattering of MDCK cells (3) in combination with PY proteomics. We identified phosphorylation of annexin A2 (AnxA2) as the major event preceding Src kinase-induced actin remodeling and cell scattering. Annexins are a large family of Ca^{2+}-binding proteins characterized by their ability to interact with negatively charged membrane surfaces (8). Structurally, annexins consist of a conserved carboxy-terminal core domain and a variable N-terminal domain. For AnxA2, this N-terminal tail domain harbors a highly specific binding site for the small dimeric protein S100A10 and phosphorylation sites for different kinases (e.g., Ser25 for protein kinase C [PKC] phosphorylation and Tyr23 for Src kinase phosphorylation) (12, 22). Recent RNA interference approaches indicate a role for AnxA2 in regulating endocytotic and exocytotic processes, as well as cell-cell junction formation and actin dynamics (14, 17, 19, 35, 39). AnxA2 and the close family member AnxA1 bind F-actin (28). For AnxA2, bundling of F-actin is regulated by S100A10-mediated tetramer formation (1, 7, 32). Src kinase-mediated phosphorylation of this AnxA2 tetrameric complex completely inhibits its ability to bind or bundle F-actin in biochemical assays (16). This suggests that Src-dependent phosphorylation of AnxA2 may regulate the cytoskeletal dynamics necessary for Src-dependent processes, such as cell scattering and EMT. Thus far, the role and mechanism of tyrosine-phosphorylated AnxA2 in the regulation of cell-cell adhesions and F-actin

* Corresponding author. Mailing address: Division of Toxicology, Leiden/Amsterdam Center for Drug Research, Gorlaeus Laboratoria, P.O. Box 9502, 2300 RA Leiden, The Netherlands. Phone: 31-71-5276223. Fax: 31-71-5274277. E-mail: b.water@lacdr.leidenuniv.nl.

† Supplemental material for this article may be found at http://mcb.asm.org/.

▽ Published ahead of print on 10 December 2007.

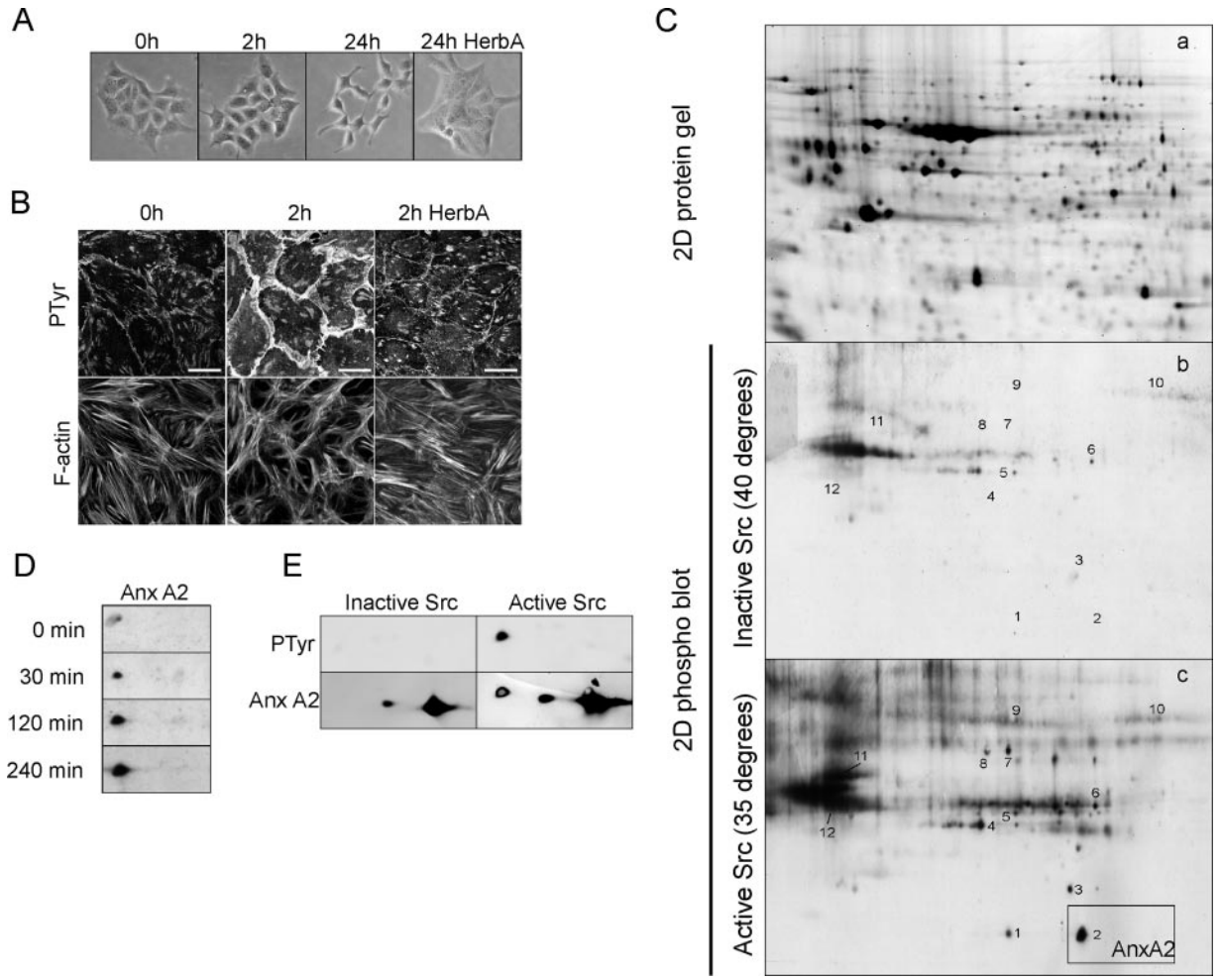

FIG. 1. Phosphoproteomic identification of AnxA2 as a phospho-substrate in Src kinase-induced scattering. *ts*-v-Src MDCK cells were shifted from the nonpermissive temperature (40°C) to the permissive temperature (35°C) for 0, 2, and 24 h in the absence or presence of herbimycin A (HerbA; 1 μM). Cells were imaged by phase-contrast microscopy (A) and immunostained for pTyr (PY99) and F-actin, followed by confocal laser scanning microscopy (B). Bars, 20 μm. For all cell lysates (40°C and 2 h at 35°C), four 2D gels were run, one preparative Sypro ruby-stained protein gel (a) and three gels for the transfer of proteins to nitrocellulose membranes and staining for pTyr proteins (b and c). All blots were analyzed with PDQuest software, followed by spot picking and MALDI-TOF MS identification of corresponding spots from Sypro ruby-stained gels (see also Table 1) (C). Phosphorylation of AnxA2 was followed in time (D). 2D blots were reprobed for AnxA2 to determine the amount of phospho-AnxA2 (E).

organization in the context of cell scattering and EMT are not known.

Here we determined the role and mechanism of tyrosine-phosphorylated AnxA2 in cell scattering and EMT-related processes. We observed that expression of a phospho-mimicking mutant form of AnxA2 (Y23E-AnxA2) is sufficient to induce F-actin reorganization and enhance cell scattering and protrusion formation, as well as formation of tubules in a branching morphogenesis assay, independently of HGF. AnxA2 was also required for cell scattering and tubulogenesis. Y23E-AnxA2 induced dephosphorylation (i.e., activation) of the actin-severing protein cofilin, whereas active LIM kinase (LIMK) inhibited AnxA2 phosphorylation-mediated cell scattering. Our results indicate a role for AnxA2 phosphorylation in the regulation of cofilin activity in the context of both 2D and 3D cellular restructuring processes.

MATERIALS AND METHODS

Cell treatment conditions. Madin-Darby canine kidney (MDCK) cells were maintained in Dulbecco modified Eagle medium supplemented with 10% (vol/vol) fetal calf serum and penicillin-streptomycin at 37°C in a humidified atmosphere of 95% air and 5% carbon dioxide. The *ts*-v-Src MDCK cell line was generated by R. Friis (3). For experiments, these cells were cultured at 40°C for 20 h and shifted to 35°C for 0 to 24 h to activate Src kinase. For preparation of stable annexin A2-expressing cell lines or short hairpin RNA (shRNA) cell lines, MDCK cells were transfected with 0.8 μg DNA of pGFP, pGFP-AnxA2 WT (wild type), and pGFP-AnxA2 Y23E (gift from V. Gerke, Institute of Medical Biochemistry, Muenster, Germany), pSUPER-empty, pSUPER-shAnxA2 non-targeting, or pSUPER-shAnxA2 (sequence A, TGACGCTTCTGAACTGAAA; sequence B, GAACTTGCATCAGCATTGA) by using Lipofectamine-Plus reagent according to the manufacturer's (Life Technologies, Inc.) procedures. Stable transfectants were selected with 800 μg/ml G418. Individual clones were picked and maintained in complete medium containing 100 μg/ml G418. Clones were analyzed for AnxA2 and green fluorescent protein (GFP) expression by Western blotting and immunofluorescence. For further experiments, up to three stable cell lines were used per construct.

TABLE 1. Data analysis of phosphoproteins and MS-based protein identifications[a]

Spot no.	Protein name	pI	Molecular mass (kDa)	NCBI accession no.	Mascot score	No. of peptides	% Sequence coverage	Species	Remark
1	Annexin A1	6.64	38.5	gi 73946797	175	17	46	*C. familiaris*	
2	Annexin A2	7.56	38.4	gi 50950177	160	15	46	*C. familiaris*	
3	Heat shock protein 60	7.4	60.1	gi 74005074	110	12	27	*C. familiaris*	
3	Ribonucleoprotein K	7.67	51.2	gi 57112247	64			*C. familiaris*	Identified with MS/MS of *m/z* 1,194.7 (NLPLPPPPPPR)
4	Cytokeratin 19	5.05	44.1	gi 6680606	54			*H. sapiens*	Identified with MS/MS of *m/z*
5	Cytokeratin 8	5.52	53.5	gi 73996455	176	19	46	*C. familiaris*	1,365.6 (SRLEQEIATYR)
6	t-complex protein zeta	5.86	60.3	gi 73957579	100	11	27	*C. familiaris*	
7	Ezrin	5.94	69.4	gi 73945736	163	22	35	*C. familiaris*	
8	Ezrin	6.03	68.6	gi 73945736	125	17	28	*C. familiaris*	
9	Vinculin	5.51	123.6	gi 4507877	88	12	17	*H. sapiens*	
10	Elongation factor 2	6.41	95.3	gi 73987435	80	10	19	*C. familiaris*	
11	Glucose-regulated protein78	5.07	72.3	gi 73968066	271	23	48	*C. familiaris*	
12	Vimentin	5.06	53.7	gi 73948960	216	19	44	*C. familiaris*	

[a] Proteins were identified by MALDI-TOF peptide mass fingerprinting. Two peptide mass fingerprints (spots 3 and 4) resulted in insignificant Mascot scores. The highest signals in these spectra were selected for MS/MS analysis and identified as peptides from ribonucleoprotein K and cytokeratin 19, respectively.

1D and 2D gel electrophoresis and Western blotting. 1D gel electrophoresis was performed as described previously (5). For 2D protein separation, 24-cm immobilized pH gradient (IPG) strips (pH 3-10 NL; GE Healthcare) were rehydrated with protein samples (obtained as described previously [5]) at 30 V for 12 h. Isoelectric focusing was performed at room temperature with the Ettan IPGphor IEF system (GE Healthcare), and IPG strips were equilibrated for 10 min in equilibration buffer (6 M urea, 2% [wt/vol] sodium dodecyl sulfate [SDS], 1% [wt/vol] DTT, 30% [vol/vol] glycerol, 50 mM Tris [pH 6.8]). Equilibrated IPG strips were subjected to 9% SDS-polyacrylamide gel electrophoresis (gel size, 20 by 26 cm). Gels were run overnight in a Hoefer DALT 10 gel system (GE Healthcare) and either fixed in 30% methanol–7.5% acetic acid for subsequent Sypro ruby staining (Molecular Probes) or transferred to nitrocellulose membrane (Schleicher & Schuell) overnight at 4°C. Both 1D and 2D blots were incubated with primary antibody overnight at 4°C with GFP (Roche), PY99 (Santa Cruz), or AnxA2 (HH7; V. Gerke), followed by incubation with horseradish peroxidase-conjugated secondary antibody for 1 h. Protein signals were detected by the ECL plus method (GE Healthcare), followed by scanning of the blots with a Typhoon 9400 (GE Healthcare).

2D image analysis and mass spectrometry. Differences in tyrosine phosphorylation were detected by PDQuest 2D gel analysis software (Bio-Rad Laboratory, Inc.). All PY profiles were aligned with total protein profiles (Sypro ruby images) to mark proteins undergoing changes in tyrosine phosphorylation. Matched spots from triplicate blots that could be detected on the associated Sypro ruby-stained gel were excised from the gel and digested with trypsin as described before (30). Tryptic digests were analyzed by matrix-assisted laser desorption ionization–time of flight mass spectrometry (MALDI-TOF MS) on an Ultraflex I (Bruker Daltonics) equipped with a LIFT-MS/MS (tandem MS) facility controlled by the FlexControl 2.0 software package. Peptide mass fingerprints and MS/MS spectra were searched against the mammalian NCBI database with the Mascot search algorithm (http://www.matrixscience.com).

Immunofluorescence. Immunofluorescence was performed as described previously (5). Cells were stained for β-catenin (Transduction Lab), PY418-Src (BioSource), PY99 (Santa Cruz), or myc (Roche) overnight at 4°C and subsequently incubated with an Alexa-488- or Cy-3-conjugated secondary antibody (Molecular Probes) in combination with rhodamine-phalloidin (Molecular Probes) to label the F-actin cytoskeletal network.

Scattering assay. For a scattering assay, cells (either left untransfected or transiently transfected) were cultured in serum-free Dulbecco modified Eagle medium overnight to form small clusters on Cn-coated coverslips. Cells were than stimulated with 50 ng/ml HGF for 7 to 10 h (50 ng/ml; Moher B.V.) to induce scattering. Thereafter, cells were fixed and stained for immunofluorescence. Scattering was quantified by measuring the percentage of cells with an epithelial (nonscattered), scattered, or highly scattered phenotype (see Fig. 4C).

GTPase activity assay. Cells were seeded on Cn-coated dishes. At 24 h after adhesion, cells were washed with ice-cold phosphate-buffered saline (containing 0.5 mM $MgCl_2$ and 1 mM $CaCl_2$) and incubated for 5 min on ice in 750 μl lysis buffer (50 mM Tris-HCl [pH 7.4], 10 mM $MgCl_2$, 1% NP-40, 10% glycerol, 100 mM NaCl, 1 mM benzamidine, 1 μg/μl leupeptin, 1 μg/μl pepstatin, 1 μg/μl aprotinin) containing GST fusion protein of the Rho-binding domain of the Rho effector protein rhotekin. Active RhoA complexes were precipitated by centrifugation, solubilized in SDS sample buffer, and analyzed by Western blotting with anti-RhoA antibody (BD Transduction Laboratories).

Live-cell imaging. For live-cell imaging, WT-AnxA2-GFP and Y23E-AnxA2-GFP cells were plated on tissue culture dishes containing a Cn-coated coverslip and maintained at 37°C in 5% CO_2 in a climate control unit on a Nikon Eclipse TE2000-U inverted microscope. Images were typically taken at 5-min interval with a Bio-Rad Radiance 2100 confocal system with a 60× Plan Apo (NA 1.4; Nikon) objective lens. Image acquisition was controlled with the Laser Sharp software (Bio-Rad) in combination with an in-house-developed macro to avoid the autofocus problem. Movies were processed with Image-Pro Plus (Version 5.1; Media Cybernetics).

Statistical analysis. Student's *t* test was used to determine if there was a significant difference between two means ($P < 0.05$). When multiple means were compared, significance was determined by one-way analysis of variance ($P < 0.05$). Significant differences are marked in the graphs.

RESULTS

Phosphoproteomics of *ts*-v-Src cells identifies phosphorylation of AnxA2 as a primary event in cell scattering. Using phosphoproteomics, we identified proteins that are differentially phosphorylated in relation to *ts*-v-Src-induced and tyrosine kinase-dependent cell-cell dissociation and scattering (3) (Fig. 1A and B). To identify potential candidate cell scattering-modifying proteins, we screened for proteins that were tyrosine phosphorylated prior to v-Src-induced loss of AJs. Therefore, PY protein blots of cells cultured at 40°C (nonpermissive) and 35°C for 2 h (permissive) were compared (Fig. 1C). Twenty-five protein spots with increased pTyr were detected. Twelve spots were positively identified by MALDI-TOF MS (Table 1), and they included (i) the transcription-regulatory proteins ribonucleoprotein K and elongation factor 2; (ii) the chaperone proteins heat shock protein 60 and GRP-78; and (iii) the cytoskeleton regulatory proteins ezrin, cytokeratins 8 and 19, t-complex protein, annexin A1 (AnxA1), annexin A2 (AnxA2), vinculin, and vimentin. AnxA2, ezrin and vinculin are known Src substrates (10, 15, 22, 27), indicating the functionality of the phosphoproteomic analysis technique. The majority of the identified proteins are involved in the regulation of the F-actin cytoskeleton. Although multiple actin-regulatory proteins were identified as differentially phosphorylated proteins 2 h after Src activation, tyrosine phosphor-

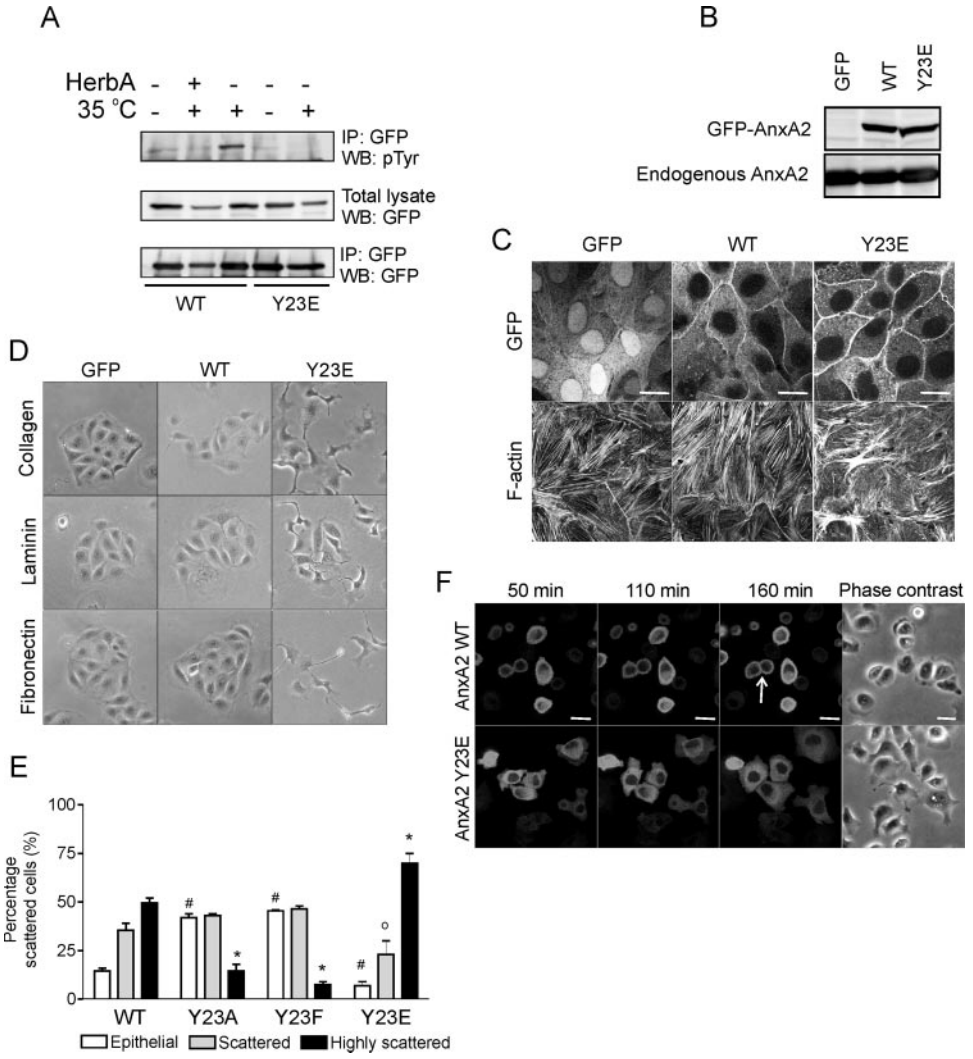

FIG. 2. Y23E-AnxA2 enhances cell spreading, protrusion formation, and cell scattering. *ts*-v-Src MDCK cells were transiently transfected with WT-AnxA2-GFP or Y23E-AnxA2-GFP and shifted to the permissive temperature (35°C) for 2 h. GFP immunoprecipitation (IP) was performed, and Western blots (WB) were stained for pTyr and GFP to determine the phosphorylation of AnxA2 (A). In addition, MDCK cells were stably transfected with GFP, WT-AnxA2-GFP, or Y23E-AnxA2-GFP. Cells were analyzed by Western blotting and AnxA2 staining (B) or plated on Cn-coated coverslips in the absence of serum and, after 24 h, fixed and imaged for GFP, AnxA2, and F-actin by confocal laser scanning microscopy (C). Bars, 20 μm. Cells were grown on Cn, Fn, or Ln at low density overnight in the absence of FBS and imaged by phase-contrast microscopy (D). To determine the involvement of phospho-AnxA2 in HGF-induced cell scattering, MDCK cells were transiently transfected with WT-, Y23A-, Y23F-, and Y23E-AnxA2-GFP and exposed to HGF for 7 h. Cell scattering was determined as described in the legend to Fig. 4. The symbols #, o, and ∗ denote statistically significant differences compared to WT-AnxA2 cells at $P < 0.05$ (E). To study cellular dynamics, live-cell imaging was performed during the first 3 h of cell adhesion (F; see Movies S1 and S2 in the supplemental material). Bars, 20 μm. Data are representative of three independent experiments.

ylation of AnxA2 was the primary and major phosphorylation event occurring within 30 min of Src activation (data not shown; Fig. 1D). Reprobing of 2D blots for AnxA2 indicated that approximately 10% of the total AnxA2 was phosphorylated in response to Src activation (Fig. 1E).

Y23E-AnxA2 increases cell scattering and protrusiveness in MDCK cells. The increase in Src-induced tyrosine phosphorylation of AnxA2 (Fig. 1E) takes place on Tyr23 (22) (Fig. 2A). Transient transfection of *ts*-v-*src* MDCK cells with WT-AnxA2 and Y23E-AnxA2, in which the Tyr residue was replaced with a Glu residue, thereby creating a phospho-mimicking mutant, showed the absence of a tyrosine-phosphorylated band in Y23E-AnxA2-expressing cells, indicating that no additional Tyr residues present in AnxA2 are targeted by Src kinase. To study the effect of phosphorylated AnxA2 on cell scattering and EMT-related processes, we generated MDCK cells that expressed low levels of WT-AnxA2 or Y23E-AnxA2 (Fig. 2B). When cells were cultured at high density, WT-AnxA2 and Y23E-AnxA2 were both associated with the plasma membrane at sites of cell-cell interaction (Fig. 2C). The F-actin network of cells expressing WT-AnxA2 resembled that of control GFP-expressing cells where F-actin stress fibers were clearly visible, while Y23E-AnxA2 cells contained fewer F-actin stress fibers and those present were short, disorganized, and often clustered

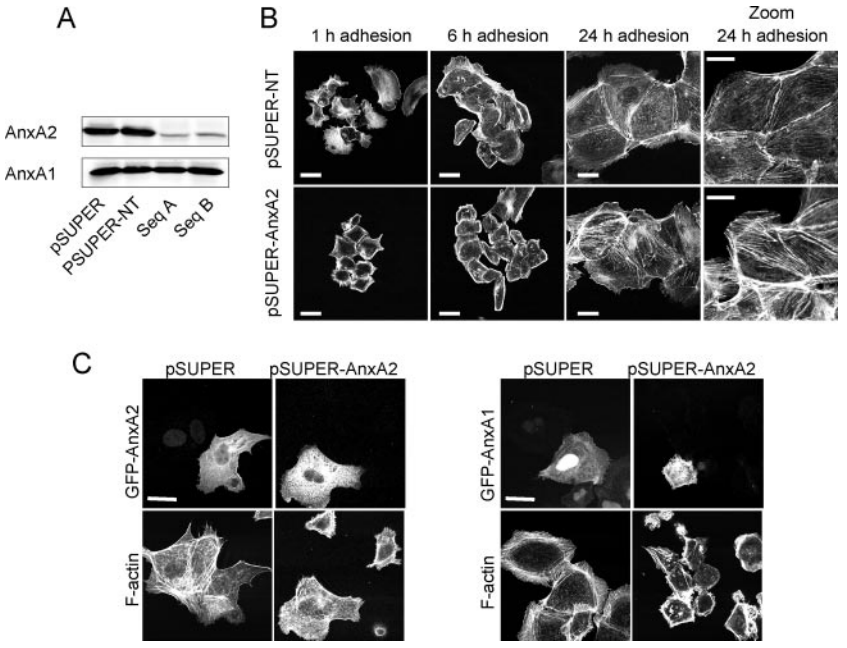

FIG. 3. AnxA2 is essential for cell spreading. MDCK cells were stably transfected with pSUPER shRNA vectors against AnxA2 (Seq A and Seq B), a pSUPER empty-vector control, or nontargeting shRNA against AnxA2 and analyzed for AnxA2 and AnxA1 expression by Western blotting (A). Three clones for each construct (pSUPER control, pSUPER-NT, and pSUPER-AnxA2 sequences A and B) were selected and pooled and used for further analysis. pSUPER-NT and pSUPER-AnxA2 cells were allowed to adhere and spread on Cn for 1, 6, and 24 h; cells were fixed and stained for F-actin, followed by confocal laser scanning microscopy. Bars, 20 μm (B). pSUPER-AnxA2 cells were transiently transfected with WT-AnxA2-GFP or WT-AnxA1-GFP, followed by spreading of the cells on Cn-coated coverslips for 2 h; cells were fixed and stained for F-actin with rhodamine-phalloidin (C). Bars, 20 μm. Data are representative of three independent experiments.

(Fig. 2C). This suggests an involvement of phosphorylated AnxA2 in the regulation of F-actin organization and dynamics (see further below).

To investigate the role of phosphorylated AnxA2 in cell scattering, Y23E-AnxA2 cells were cultured overnight at low density on Cn, fibronectin (Fn), or laminin (Ln). GFP and WT-AnxA2 cells formed small islets on all three extracellular matrix substrates. In contrast, Y23E-AnxA2 cells obtained a scattered morphology resembling that of Src kinase- or HGF-induced scattering (Fig. 2D, compare with 1A and 4D). Scattering was enhanced on Cn and Fn, compared to Ln, suggesting an involvement of specific integrin-mediated signaling in the Y23E-AnxA2-induced scattering. In addition, treatment of cells expressing WT-AnxA2, Y23E-AnxA2, or one of the phospho-defective mutants Y23A-AnxA2 and Y23F-AnxA2 with the scatter factor HGF showed an involvement of phospho-AnxA2 in the regulation of cell scattering downstream of growth factor signaling. While Y23E-AnxA2 enhanced cell scattering induced by HGF, the phospho-defective mutants inhibited cell scattering (Fig. 2E).

To determine whether the scattered phenotype of Y23E-AnxA2 cells is associated with the formation of dynamic protrusions early during spreading, live-cell imaging was performed (Fig. 2F; see Movies S1 and S2 in the supplemental material). Y23E-AnxA2 cells obtained a scattered phenotype early after adhesion, with the formation of many dynamic lamellipodia per cell (see Movie S2 in the supplemental material; Fig. 2F). This did not occur in WT-AnxA2 cells (see Movie S1 in the supplemental material; Fig. 2F). In some cells, Y23E-AnxA2 localized in newly formed lamellipodia. In contrast to WT-AnxA2-expressing cells, which readily formed new cell-cell junctions, Y23E-AnxA2-expressing cells did not, despite the fact that these cells were in close proximity. Together, these data show that Y23E-AnxA2 by itself stimulates cell spreading and generation of dynamic lamellipodia and most likely prohibits the formation of stable cell-cell junctions when cells are cultured at low density.

Cell spreading and scattering are inhibited by AnxA2 knockdown and depend on tyrosine phosphorylation of AnxA2. Since Y23E-AnxA2 caused cell scattering, we anticipated a functional role for AnxA2 itself in cell spreading and scattering. To study this, we generated AnxA2 knockdown MDCK cells with shRNA. Compared to empty-vector control cells (pSUPER) or cells expressing a nontargeting AnxA2 shRNA (pSUPER-NT), the levels of AnxA2 were greatly reduced in cells expressing two independent shRNA sequences (pSUPER-AnxA2 sequences A and B) while a close family member, AnxA1, was unaffected (Fig. 3A). While Y23E-AnxA2 enhanced cell spreading (Fig. 2), AnxA2 knockdown inhibited early cell spreading (Fig. 3B) and, compared to pSUPER-NT cells, showed a strong cortical actin network at 1 and 6 h after adhesion. At 24 h, pSUPER-AnxA2 cells were fully spread and formed small islets, similar to pSUPER-NT cells. However, AnxA2 knockdown was associated with a thicker and denser F-actin stress fiber network (Fig. 3B, zoom). The early defects in cell spreading were rescued by expression of WT-AnxA2 but not AnxA1 (Fig. 3C).

To determine the role of AnxA2 in cell scattering, *ts*-vSrc MDCK cells were transiently transfected with the pSUPER or pSUPER-AnxA2 vector (sequences A and B). Compared to the

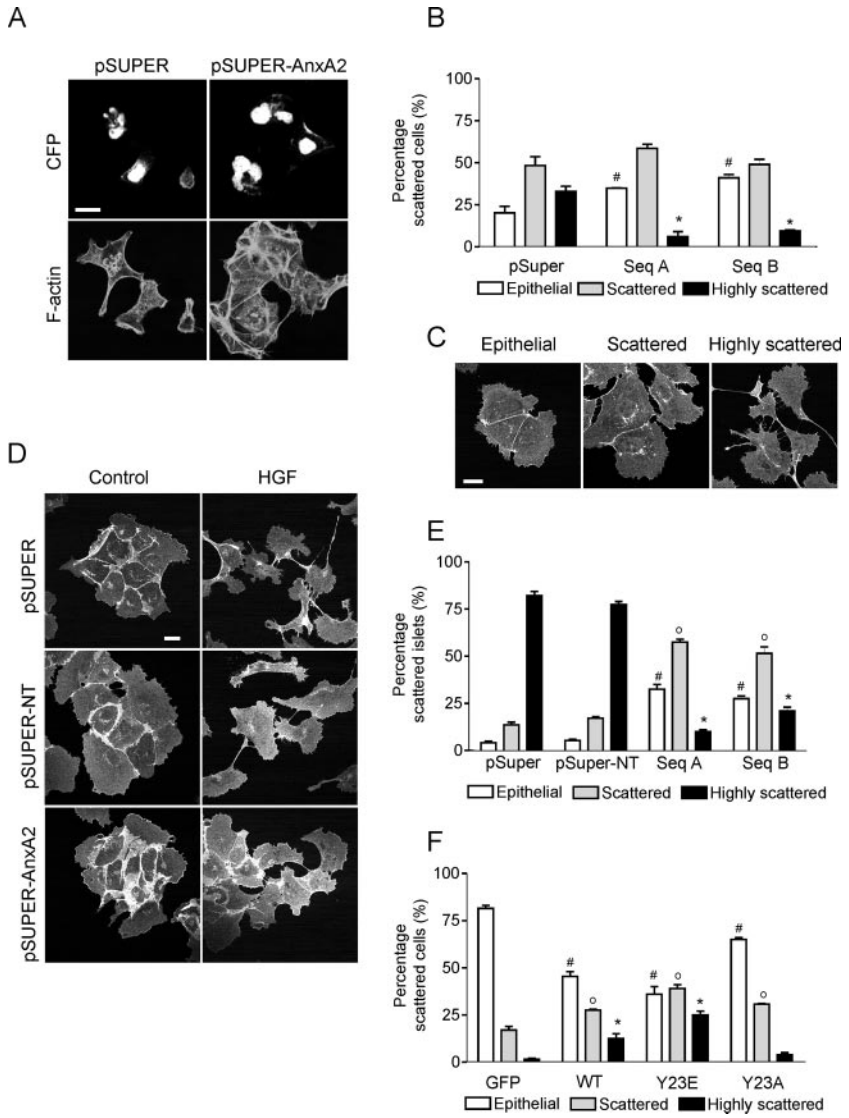

FIG. 4. Cell scattering is inhibited by AnxA2 knockdown and depends on tyrosine phosphorylation of AnxA2. *ts*-v-Src MDCK cells were transiently transfected with a pSUPER control and pSUPER-AnxA2 sequences A and B. Cells were shifted to the permissive temperature for 4 h, stained for F-actin, and imaged by confocal laser scanning microscopy (A and B). Cell scattering was quantified by counting the cyan fluorescent protein-histone 2B (sSUPER)-positive epithelial (0% loss of cell-cell interaction), scattered (<50% loss of cell-cell interaction), and highly scattered (>50% loss of cell-cell interaction) cells (C). Stably transfected cells expressing pSUPER, pSUPER-NT, or pSUPER-AnxA2 (sequences A and B) were exposed to HGF (50 ng/μl) for 10 h (D and E). Cell scattering was determined by the percentage of islets with epithelial, scattered, or highly scattered cells (E). pSUPER-AnxA2 cells were transiently transfected with HA-tagged CA-Src kinase in combination with GFP, WT-AnxA2, Y23E-AnxA2, or Y23A-AnxA2 in the absence of serum. Cell scattering was determined as for panel C, by counting GFP-positive cells (F). Data are representative of three independent experiments. Bars, 20 μm. The symbols #, o, and ∗ denote statistically significant differences compared to either pSUPER or GFP cells at $P < 0.05$.

levels of AnxA2 in cells expressing the empty vector (pSUPER), they were reduced in cells expressing either shRNA sequence A or B (pSUPER-AnxA2) (data not shown). Cell scattering was quantified by scoring the percentage of cells with an epithelial (nonscattered), scattered, or highly scattered phenotype (Fig. 4C). Expression of pSUPER-AnxA2 (either sequence A or sequence B) reduced the number of highly scattered cells but did not block cell scattering completely (Fig. 4A and B). In addition to the inhibition of v-Src-induced cell scattering, AnxA2 knockdown decreased cell scattering induced by the scatter factor HGF in normal MDCK cells (Fig. 4D and E). These data indicate that AnxA2 is important for the regulation of cell spreading and scattering.

To determine whether cell scattering depends on the tyrosine phosphorylation of AnxA2, pSUPER-AnxA2 cells were transiently transfected with constitutively active Src kinase to induce cell scattering, in combination with enhanced GFP (EGFP), WT-AnxA2, Y23E-AnxA2, and Y23A-AnxA2. Compared to EGFP, WT-AnxA2 increased Src-induced cell scattering of pSUPER-AnxA2 cells (Fig. 4F). Strikingly, while Y23E-AnxA2 even further increased the percentage of (highly) scattered cells, expression of the phospho-defective

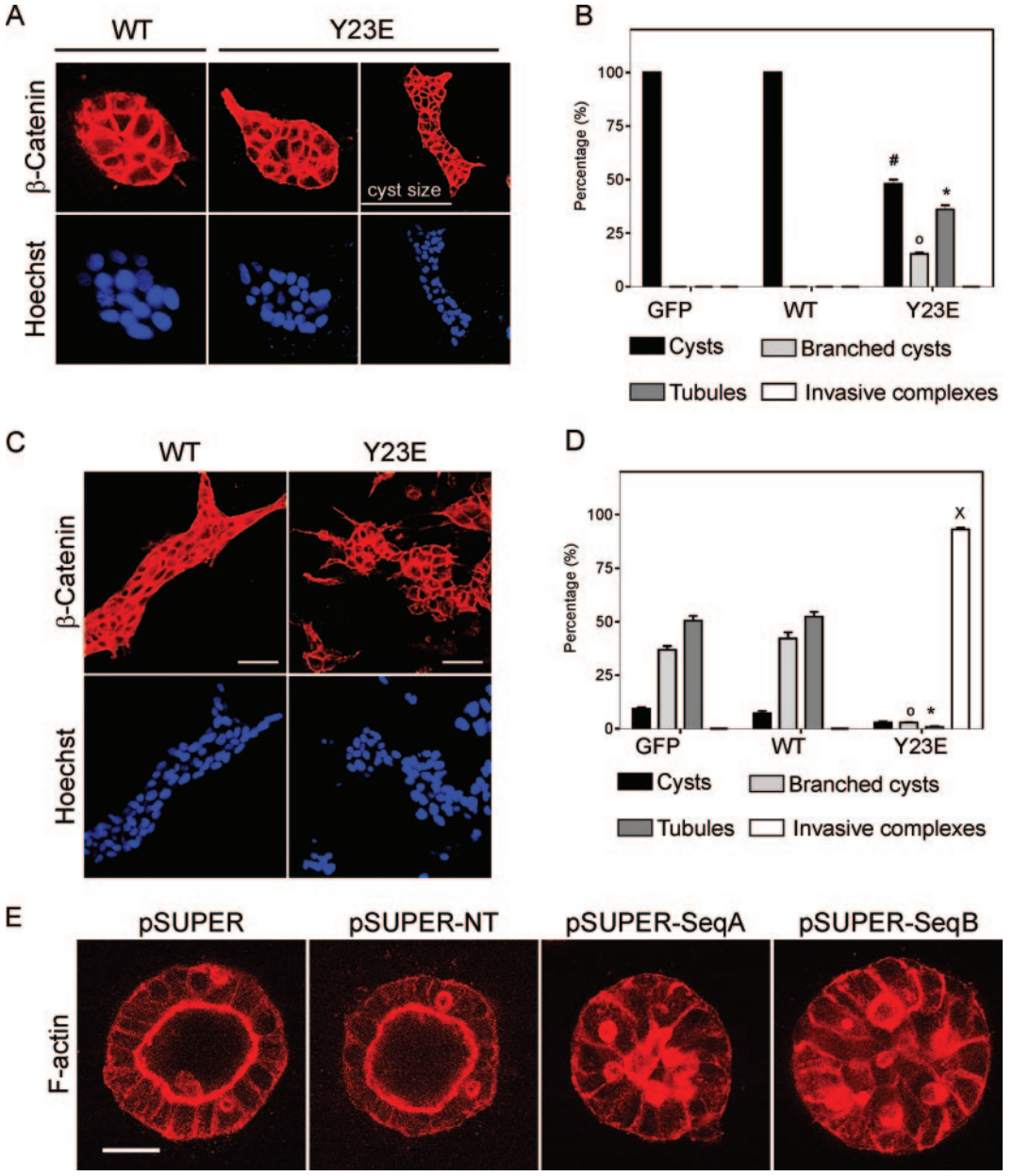

FIG. 5. Y23E-AnxA2 induces HGF-independent branching morphogenesis. GFP, GFP-WT-AnxA2, and GFP-Y23E-AnxA2 cells were assayed for branching morphogenesis in a 3D Cn type 1 gel. To determine the shape of the 3D complexes, β-catenin and Hoechst staining were used. Nonstimulated cells (A) and HGF-stimulated cells (C) were analyzed by confocal laser scanning microscopy after 7 days of growth. Bars, 50 μm. The percentages of cysts, branched complexes, tubules, and invasive complexes were determined for nonstimulated control cells (B) and for HGF-stimulated cells (D). pSUPER, pSUPER-NT, and pSUPER-AnxA2 (sequences A and B) cells were cultured in a 3D Cn I–10% Matrigel gel for 7 days and, after fixation, stained for F-actin and β-catenin. Bars, 20 μm (E). In panels B and D, the data represent the mean ± the standard error of the mean of two independent experiments including two different clones for GFP-, GFP-WT-AnxA2-, and GFP-Y23E-AnxA2-expressing cells. The symbols #, o, *, and × denote significant differences compared to WT-AnxA2 cells at $P < 0.05$.

mutant Y23A-AnxA2 decreased the percentage of highly scattered cells. Thus, cell scattering depends on the phosphorylation of AnxA2.

Y23E-AnxA2 triggers a 3D branching morphogenesis process. The scattering phenotype associated with the expression of Y23E-AnxA2 is reminiscent of the scattered/mesenchymal phenotype that is also observed with HGF. EMT processes are essential for the formation of multicellular structures (25). Since HGF induces a 3D branching morphogenesis process in MCDK cells when they are cultured in Cn gels, we reasoned that Y23E-AnxA2 itself would also mediate such a process. As expected, only round cysts were observed with WT-AnxA2 cells and GFP control cells in the absence of HGF. In contrast, ~20% of the Y23E-AnxA2 cysts contained membrane protrusions on the outside while ~30% of the cysts derived from Y23E-AnxA2 cells spontaneously developed into tubules (Fig.

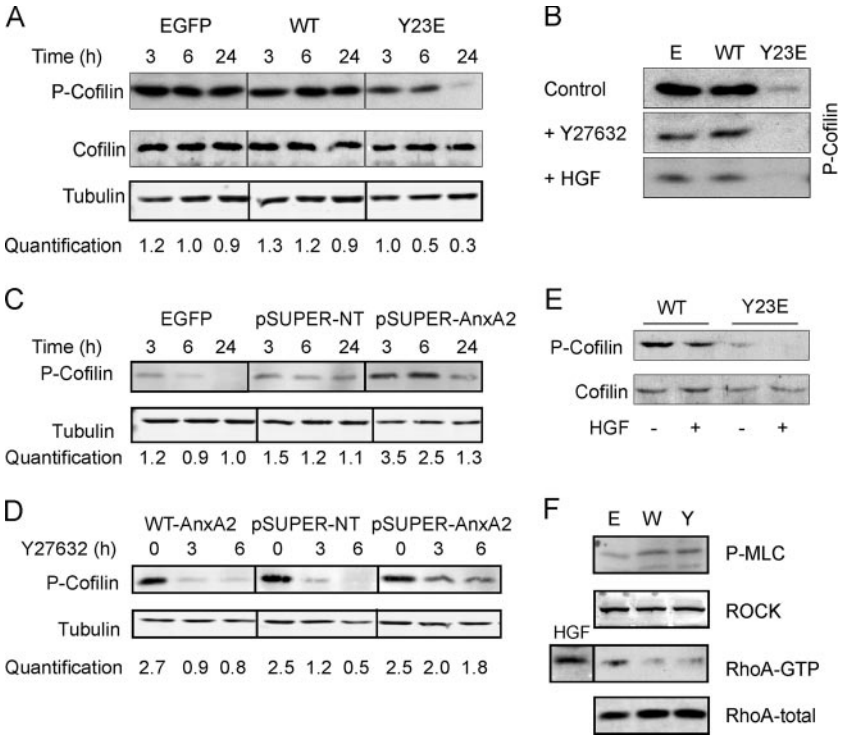

FIG. 6. Y23E-AnxA2 activates the actin-severing protein cofilin via dephosphorylation. EGFP, WT-AnxA2, and Y23E-AnxA2 cells were cultured and allowed to spread on Cn for 3, 6, or 24 h (A) or grown in a branching morphogenesis assay (E) and analyzed for cofilin phosphorylation by Western blotting. To decrease cofilin phosphorylation, cells were cultured on Cn for 24 h and thereafter treated with HGF (50 ng/ml) or the ROCK inhibitor Y27632 (10 μM) for 10 h (B). pSUPER-NT and pSUPER-AnxA2 cells were cultured and allowed to spread on Cn for 3, 6, or 24 h (C) and thereafter exposed to the ROCK inhibitor Y27632 for 3 and 6 h (D) to determine cofilin phosphorylation. Phosphorylation of cofilin is quantified (A, C, and D) and shown below the blot as a ratio of the phospho-cofilin/tubulin staining for three independent experiments. To determine the levels of phosphorylated myosin light chain (P-MLC) and ROCK and the activation status of RhoA, cells were allowed to spread for 24 h and thereafter analyzed by Western blotting (F). RhoA activation was determined by a RhoA pull-down assay as described in Materials and Methods (F). Data are representative of three independent experiments. The different blots shown were derived from the same blot and have the same exposure time.

5A and B). Stimulation of 3-day-old WT-AnxA2 cysts with HGF resulted in the formation of tubules (Fig. 5C and D). In Y23E-AnxA2 cells, no tubule structures were observed after HGF treatment, but rather large invasive cellular complexes were formed with randomly distributed cellular protrusions (Fig. 5C and D). AnxA2 knockdown almost completely prevented cyst formation in a Cn gel (data not shown), possibly because these cells had difficulties in adhering to the Cn matrix and subsequently proliferated and survived. Yet, addition of 10% Matrigel to the Cn gels greatly improved the formation of pSUPER-AnxA2 3D spheroids since cells adhered better to this mixture of matrices during the first day in a 3D environment, possibly stimulating proper proliferation. While control cells formed a polarized lumen under these conditions, AnxA2 knockdown prevented lumen formation during cystogenesis (Fig. 5E). Since Matrigel itself prevented HGF branching morphogenesis of both control and pSUPER-AnxA2 cells, we were unable to further follow branching morphogenesis under these conditions. Together, these data underscore the requirement for AnxA2 in 3D branching morphogenesis processes and establish that phosphorylation of AnxA2 on Tyr23 itself can drive the branching morphogenesis process in the absence of HGF and further cooperates with HGF to induce an advanced invasive branched phenotype.

Dephosphorylation of the actin-severing protein cofilin in Y23E-AnxA2 cells controls cell scattering and branching morphogenesis. Y23E-AnxA2 induced lamellipodium formation and increased cellular dynamics, while actin stress fiber formation was reduced. The formation and contractility of stress fibers are regulated by activation of the Rho kinase (ROCK) pathway through downstream modulation of cofilin, an actin-severing protein and terminal effector of the ROCK pathway. Therefore, we reasoned that the Y23E-AnxA2-induced scattering was directly related to the modulation of cofilin. Indeed, during cell adhesion and spreading, cofilin phosphorylation was lower in Y23E-AnxA2 cells compared to WT-AnxA2 cells (Fig. 6A) and almost completely absent after 24 h of adhesion when Y23E-AnxA2 had obtained a scattered phenotype (Fig. 2B). The levels of cofilin phosphorylation in scattered Y23E-AnxA2 cells resembled those in WT-AnxA2 cells in which scattering was induced by HGF or the ROCK inhibitor Y27632 (Fig. 6B). To asses the ability of AnxA2 to mediate cofilin phosphorylation, next the cofilin phosphorylation status was determined in pSUPER-AnxA2 cells (sequence B). Early during cell adhesion and spreading, when pSUPER-AnxA2 showed a decrease in cell spreading (Fig. 3B), cofilin phosphorylation levels were increased compared to those in control cells (Fig. 6C). Since Y23E-AnxA2 itself causes branching morpho-

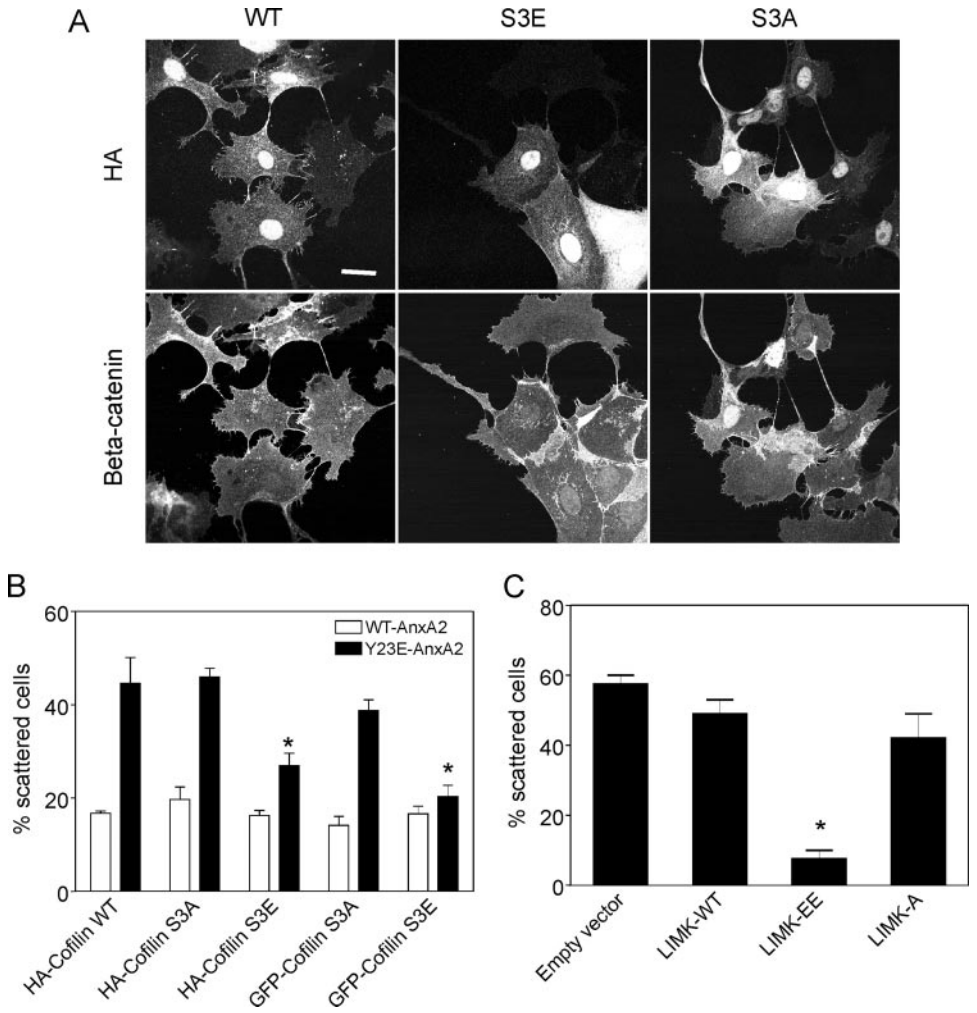

FIG. 7. Phospho-mimicking cofilin and constitutively active LIMK rescue Y23E-AnxA2-induced scattering. WT-AnxA2 and Y23E-AnxA2 cells were transiently transfected with HA-WT-, HA-S3A-, or HA-S3E-cofilin and alternatively with GFP-S3A- or GFP-S3E-cofilin (A and B) or the empty vector, HA-LIMK-WT, HA-LIMK-T508EE, or HA-LIMK-T508A (C). After plating on Cn overnight, cells were fixed and stained for F-actin, followed by confocal laser scanning microscopy imaging of the both GFP and rhodamine-phalloidin and quantification of the percentage of scattered cells. Data are the mean ± the standard error of the mean of two independent experiments, with 50 to 100 counted cells per experiment. Asterisks denote significant differences compared to HA-cofilin WT or empty-vector control cells at $P < 0.05$.

genesis in 3D, we anticipated that Y23E-AnxA2 also affected cofilin phosphorylation in 3D cultures. Indeed, in Y23E-AnxA2 tubules, cofilin phosphorylation was reduced compared to that in WT-AnxA2 cysts (Fig. 6E). While cofilin phosphorylation levels were slightly reduced in HGF-treated WT-AnxA2, almost no phosphorylation of cofilin was observed in the invasive 3D structures caused by combined Y23E-AnxA2 expression and HGF treatment (Fig. 6E).

Since cofilin phosphorylation is regulated upstream via activation of the Rho/ROCK pathway, we determined whether AnxA2 and its phosphorylation could affect this pathway. While inhibition of ROCK signaling by the treatment of cells with the ROCK inhibitor Y27632 resulted in fast cofilin dephosphorylation in WT-AnxA2 and pSUPER-NT cells, cofilin dephosphorylation was delayed in AnxA2 knockdown cells (Fig. 6D). This suggests that AnxA2 is involved in the ROCK/LIMK-dependent cofilin (de)phosphorylation cycle. The activation status of the RhoA/ROCK pathway was also determined in Y23E-AnxA2 cells at 24 h after spreading, when phospho-cofilin levels were low and cell scattering was observed (Fig. 2D). Y23E-AnxA2 affected neither RhoA activation nor ROCK activation, as determined by the levels of phosphorylated myosin light chain (Fig. 6F). This suggests that AnxA2 tyrosine phosphorylation regulates cofilin phosphorylation in a RhoA/ROCK-independent way, possibly directly via regulation of LIMK activation.

Inactive cofilin and an upstream cofilin kinase, LIMK, inhibit Y23E-AnxA2-induced cell scattering. To determine the involvement of cofilin phosphorylation in the Y23E-AnxA2-mediated scattering process, Y23E-AnxA2 cells were transiently transfected with WT-cofilin, S3A-cofilin (constitutively active), or S3E-cofilin (constitutively inactive) (Fig. 7A). Both hemagglutinin (HA)- and GFP-tagged versions of these mutants were used. Expression of both the HA- and GFP-tagged versions of the S3E-cofilin mutant efficiently inhibited the scattering of Y23E-AnxA2 cells, which was associated with the

formation of cell-cell junctions (Fig. 7A and B). Y23E-AnxA2 cells expressing WT-cofilin obtained a scattered phenotype as untransfected cells (Fig. 7A and B). Neither HA- or GFP-tagged S3A cofilin nor WT-cofilin affected the cell-scattering phenotype of Y23E-AnxA2 cells. Moreover, S3A-cofilin itself did not induce scattering in WT-AnxA2 cells. Since active LIMK is able to phosphorylate cofilin, we anticipated that expression of active LIMK would inhibit Y23E-AnxA2-induced cell scattering. Indeed, expression of constitutively active LIMK (LIMK-T508EE) resulted in a major decrease in the percentage of scattered Y23E-AnxA2 cells (Fig. 7C), while expression of inactive LIMK (LIMK-T508A) had no effect on the scattering induced by Y23E-AnxA2 (Fig. 7C). Altogether, these observations indicate that tyrosine phosphorylation of AnxA2 on Tyr23 affects cofilin phosphorylation and function, possibly via LIMK inactivation, thereby allowing a continuous dynamic actin reorganization which promotes dynamic cell protrusion formation, cell scattering, and branching morphogenesis.

DISCUSSION

Formation of a scattered phenotype is a central problem in understanding both branching morphogenesis and cancer cell metastatic phenotypes. Using PY proteomics, we have identified candidate cell scattering-modifying proteins downstream of the oncogenic nonreceptor tyrosine kinase Src. Our data support a central biological role for AnxA2 phosphorylation on Tyr23 in the regulation of cell scattering and EMT-mediated processes. Thus, our results indicate that tyrosine phosphorylation of AnxA2 by itself enhances cell spreading and protrusiveness and induces cell scattering in 2D and HGF-independent branching morphogenesis in 3D. Importantly, shRNA-mediated knockdown of AnxA2 inhibited cell spreading, scattering, and normal cystogenesis. The AnxA2 tyrosine phosphorylation-driven events occurred in association with an altered F-actin cytoskeletal rearrangement in association with activation of the cofilin pathway.

Besides AnxA2, also other v-Src targets were identified. Most of these identified, differentially phosphorylated proteins are (in)directly associated with v-Src-induced cytoskeletal restructuring. Ezrin is phosphorylated on two residues, of which at least Src-induced phosphorylation of Y145 is required for the regulation of cytoskeletal reorganization prior to cell scattering (29). v-Src caused at least the phosphorylation of Y477 in MDCK cells (M. de Graauw et al., unpublished data), but the cell biological role of this phosphorylation needs further evaluation. In addition, vinculin is a direct target of Src kinase and mutation of the tyrosine residue results in impaired cell spreading (37). The close family members AnxA1 and AnxA2, which both bind F-actin, belong to the first proteins phosphorylated in relation to v-Src kinase activation. While AnxA1 has been shown to be phosphorylated by the epidermal growth factor receptor, AnxA2 has previously been identified as a direct target for Src kinase (22). The combined phosphorylation of these different cytoskeleton-associated proteins may be required for the well-coordinated reorganization and/or turnover of the actin cytoskeletal network, thereby facilitating cell scattering. However, for a large portion, the Y23E-AnxA2 phenotype mimics the v-Src-induced phenotype, suggesting that AnxA2 is not only the major tyrosine-phosphorylated protein but also a crucial player in v-Src-induced scattering.

AnxA2 is found at the membrane-actin cytoskeleton interface and is associated with sites of active actin remodeling, like rocketing macropinosomes (14, 20), actin-rich pedestals (38), and lamellipodia (26). Our data indicate that AnxA2 phosphorylation is important in actin remodeling. While Y23E-AnxA2-expressing cells showed a reduction in actin stress fiber formation, cells depleted of AnxA2 become enriched in stress fibers (Fig. 3B) (14) and are defective in the formation of a polarized cyst with an actin-rich apical domain (Fig. 4E) (18). AnxA2 localizes to regions of active actin remodeling enriched in the plasma membrane lipid phosphatidylinositol-4,5-bisphosphate PtdIns(4,5)*P2* (13, 24). The architecture of the PtdIns(4,5)*P2* binding site in AnxA2 is not precisely known but depends, at least in part, on its unique N-terminal domain since the C-terminal AnxA2 core domain does not efficiently compete with full-length AnxA2 for PtdIns(4,5)*P2* binding (11, 24). Since Tyr23 of AnxA2 is located within this region, phosphorylation apparently influences its binding to these PtdIns(4,5)*P2* sites, most likely through altered protein conformation, thereby directing AnxA2 to cellular microenvironments with high actin remodeling activity and targeting other cytoskeletal and/or morphogenesis-regulating proteins, including Cdc42 and the Par6/aPKC complex (18).

AnxA2-mediated actin remodeling is related to its ability to influence the phosphorylation status (i.e., functional activation) of the actin-severing protein cofilin. We propose that Y23E-AnxA2-induced cell scattering is directly related to cofilin dephosphorylation. Firstly, two independent constructs of the phosphorylation-mimicking cofilin S3E mutant (HA and GFP tagged) inhibited cell scattering while phospho-defective S3A did not affect scattering. Secondly, pharmacological inhibition of the ROCK/cofilin pathway with Y27632 caused cofilin dephosphorylation (Fig. 6B), loss of F-actin stress fibers and cellular tension, and increased MDCK cell scattering and uncontrolled branching morphogenesis (unpublished observation;6). Importantly, depletion of AnxA2 inhibited Y27632-induced cofilin dephosphorylation (Fig. 6F) and cell scattering (unpublished observations), indicating a role for AnxA2 in the regulation of cofilin phosphorylation. Thirdly, the Rho/ROCK/LIMK pathway has been described as a major upstream effector pathway of cofilin modulation (31, 34). Despite the fact that AnxA2 binds RhoA and thereby regulates RhoA activation in Caco-2 cells (2), in our studies with MDCK cells, Y23E-AnxA2 did not affect the activation status of RhoA upstream of cofilin. Nevertheless, expression of a constitutively active LIMK (HA-LIMK-508EE) significantly reduced the number of scattered Y23E-AnxA2 cells (Fig. 7C), suggesting that the pool of nonphosphorylated cofilin that drives the AnxA2-mediated scattering can be targeted by LIMK. Unfortunately, the potential activation of LIMK due to Y23E-AnxA2 expression could not be determined since no good working antibody was available. Together, these data support the notion that AnxA2 affects the rate of phosphorylated cofilin turnover, and thereby cell scattering, possibly by suppressing LIMK activity in a RhoA-independent manner or by activation of the cofilin phosphatase Slingshot. This needs further investigation.

Alternatively, AnxA2 may influence cofilin phosphorylation

more directly via competition of binding to actin monomers. Cofilin affects actin polymerization through its ability to sequesters actin monomers in a phosphorylation-dependent manner (4, 11). It disassembles F-actin from the rear of the actin network to recycle actin monomers to the leading edge for further rounds of polymerization, thus driving lamellipodium formation. Also, AnxA2 binds and sequesters G-actin directly, thereby regulating actin filament turnover, most likely through monomer sequestration and barbed-end capping activities (14). Phosphorylation of AnxA2 possibly affects its binding to monomers, explaining the diminished formation of stress fibers in Y23E-AnxA2 cells. In contrast, AnxA2 knockdown decreases the actin filament turnover, causing the formation of thick stress fibers. Since AnxA2 also has the ability to bind to the plasma membrane, it is able to deliver actin monomers directly to the cell cortex, where they are required for rapid polymerization.

Protein tyrosine kinases, including epidermal growth factor receptor family members and Src kinases, play an important role in cancer development and progression. This is often related to a mesenchymal/dedifferentiated phenotype of the tumor cells and a high metastatic potential. Interestingly, AnxA2 expression is elevated in a subset of metastatic breast tumor cells with a mesenchymal phenotype (M. de Graauw, A. M. Cleton-Janssen, and B. van de Water, unpublished observations). Therefore, the combination of high protein tyrosine kinase activity and high AnxA2 expression may ensure increased AnxA2 tyrosine phosphorylation, thereby driving cell scattering and supporting tumor metastasis formation. Consequently, upstream and downstream molecular programs that control and mediate the function of tyrosine-phosphorylated AnxA2 may be novel targets for therapeutic intervention.

ACKNOWLEDGMENTS

We thank V. Gerke and U. Rescher for the AnxA2 constructs and antibodies, Flip Deen for the Sypro ruby staining solution, Danny Burg for help with the shRNA constructs, and Erik Danen and other members of the Division of Toxicology of the LACDR for valuable discussion and critically reading the manuscript.

This work was supported by grants from The Netherlands Organization for Scientific Research (902-21-229 and 911-02-022) and the Dutch Cancer Foundation (2006-3538).

REFERENCES

1. **Alvarez-Martinez, M. T., J. C. Mani, F. Porte, C. Faivre-Sarrailh, J. P. Liautard, and W. J. Sri.** 1996. Characterization of the interaction between annexin I and profilin. Eur. J. Biochem. **238:**777–784.
2. **Babbin, B. A., C. A. Parkos, K. J. Mandell, L. M. Winfree, O. Laur, A. I. Ivanov, and A. Nusrat.** 2007. Annexin 2 regulates intestinal epithelial cell spreading and wound closure through Rho-related signaling. Am. J. Pathol. **170:**951–966.
3. **Behrens, J., L. Vakaet, R. Friis, E. Winterhager, F. Van Roy, M. M. Mareel, and W. Birchmeier.** 1993. Loss of epithelial differentiation and gain of invasiveness correlates with tyrosine phosphorylation of the E-cadherin/beta-catenin complex in cells transformed with a temperature-sensitive v-SRC gene. J. Cell Biol. **120:**757–766.
4. **Bershadsky, A.** 2004. Magic touch: how does cell-cell adhesion trigger actin assembly? Trends Cell Biol. **14:**589–593.
5. **de Graauw, M., I. Tijdens, R. Cramer, S. Corless, J. F. Timms, and B. van de Water.** 2005. Heat shock protein 27 is the major differentially phosphorylated protein involved in renal epithelial cellular stress response and controls focal adhesion organization and apoptosis. J. Biol. Chem. **280:**29885–29898.
6. **de Rooij, J., A. Kerstens, G. Danuser, M. A. Schwartz, and C. M. Waterman-Storer.** 2005. Integrin-dependent actomyosin contraction regulates epithelial cell scattering. J. Cell Biol. **171:**153–164.
7. **Filipenko, N. R., and D. M. Waisman.** 2001. The C terminus of annexin II mediates binding to F-actin. J. Biol. Chem. **276:**5310–5315.
8. **Gerke, V., C. E. Creutz, and S. E. Moss.** 2005. Annexins: linking Ca^{2+} signalling to membrane dynamics. Nat. Rev. Mol. Cell Biol. **6:**449–461.
9. Reference deleted.
10. **Glenney, J.** 1986. Two related but distinct forms of the M_r 36,000 tyrosine kinase substrate (calpactin) that interact with phospholipid and actin in a Ca^{2+}-dependent manner. Proc. Natl. Acad. Sci. USA **83:**4258–4262.
11. **Gokhale, N. A., A. Abraham, M. A. Digman, E. Gratton, and W. Cho.** 2005. Phosphoinositide specificity of and mechanism of lipid domain formation by annexin A2-p11 heterotetramer. J. Biol. Chem. **280:**42831–42840.
12. **Gould, K. L., J. R. Woodgett, C. M. Isacke, and T. Hunter.** 1986. The protein-tyrosine kinase substrate p36 is also a substrate for protein kinase C in vitro and in vivo. Mol. Cell. Biol. **6:**2738–2744.
13. **Hayes, M. J., C. J. Merrifield, D. Shao, J. Ayala-Sanmartin, C. D. Schorey, T. P. Levine, J. Proust, J. Curran, M. Bailly, and S. E. Moss.** 2004. Annexin 2 binding to phosphatidylinositol 4,5-bisphosphate on endocytic vesicles is regulated by the stress response pathway. J. Biol. Chem. **279:**14157–14164.
14. **Hayes, M. J., D. Shao, M. Bailly, and S. E. Moss.** 2006. Regulation of actin dynamics by annexin 2. EMBO J. **25:**1816–1826.
15. **Heiska, L., and O. Carpén.** 2005. Src phosphorylates ezrin at tyrosine 477 and induces a phosphospecific association between ezrin and a kelch-repeat protein family member. J. Biol. Chem. **280:**10244–10252.
16. **Hubaishy, I., P. G. Jones, J. Bjorge, C. Bellagamba, S. Fitzpatrick, D. J. Fujita, and D. M. Waisman.** 1995. Modulation of annexin II tetramer by tyrosine phosphorylation. Biochemistry **34:**14527–14534.
17. **Knop, M., E. Aareskjold, G. Bode, and V. Gerke.** 2004. Rab3D and annexin A2 play a role in regulated secretion of vWF, but not tPA, from endothelial cells. EMBO J. **23:**2982–2992.
18. **Martin-Belmonte, F., A. Gassama, A. Datta, W. Yu, U. Rescher, V. Gerke, and K. Mostov.** 2007. PTEN-mediated apical segregation of phosphoinositides controls epithelial morphogenesis through Cdc42. Cell **128:**383–397.
19. **Mayran, N., R. G. Parton, and J. Gruenberg.** 2003. Annexin II regulates multivesicular endosome biogenesis in the degradation pathway of animal cells. EMBO J. **22:**3242–3253.
20. **Merrifield, C. J., U. Rescher, W. Almers, J. Proust, V. Gerke, A. S. Sechi, and S. E. Moss.** 2001. Annexin 2 has an essential role in actin-based macropinocytic rocketing. Curr. Biol. **11:**1136–1141.
21. **O'Brien, L. E., M. M. Zegers, and K. E. Mostov.** 2002. Building epithelial architecture: insights from three-dimensional culture models. Nat. Rev. Mol. Cell Biol. **3:**531–537.
22. **Radke, K., and G. S. Martin.** 1979. Transformation by Rous sarcoma virus: effects of *src* gene expression on the synthesis and phosphorylation of cellular polypeptides. Proc. Natl. Acad. Sci. USA **76:**5212–5216.
23. **Rahimi, N., W. Hung, E. Tremblay, R. Saulnier, and B. Elliott.** 1998. c-Src kinase activity is required for hepatocyte growth factor-induced motility and anchorage-independent growth of mammary carcinoma cells. J. Biol. Chem. **273:**33714–33721.
24. **Rescher, U., D. Ruhe, C. Ludwig, N. Zobiack, and V. Gerke.** 2004. Annexin 2 is a phosphatidylinositol (4,5)-bisphosphate binding protein recruited to actin assembly sites at cellular membranes. J. Cell Sci. **117:**3473–3480.
25. **Rosário, M., and W. Birchmeier.** 2003. How to make tubes: signaling by the Met receptor tyrosine kinase. Trends Cell Biol. **13:**328–335.
26. **Royal, I., and M. Park.** 1995. Hepatocyte growth factor-induced scatter of Madin-Darby canine kidney cells requires phosphatidylinositol 3-kinase. J. Biol. Chem. **270:**27780–27787.
27. **Sefton, B. M., T. Hunter, E. H. Ball, and S. J. Singer.** 1981. Vinculin: a cytoskeletal target of the transforming protein of Rous sarcoma virus. Cell **24:**165–174.
28. **Shadle, P. J., V. Gerke, and K. Weber.** 1985. Three Ca^{2+}-binding proteins from porcine liver and intestine differ immunologically and physicochemically and are distinct in Ca^{2+} affinities. J. Biol. Chem. **260:**16354–16360.
29. **Srivastava, J., B. E. Elliott, D. Louvard, and M. Arpin.** 2005. Src-dependent ezrin phosphorylation in adhesion-mediated signaling. Mol. Biol. Cell **16:**1481–1490.
30. **Steen, H., A. Pandey, J. S. Andersen, and M. Mann.** 15 October 2002. Analysis of tyrosine phosphorylation sites in signaling molecules by a phosphotyrosine-specific immonium ion scanning method. Sci. STKE **2002:**L16. doi:10.1126/stke.2002.154.pl16.
31. **Sumi, T., K. Matsumoto, and T. Nakamura.** 2001. Specific activation of LIM kinase 2 via phosphorylation of threonine 505 by ROCK, a Rho-dependent protein kinase. J. Biol. Chem. **276:**670–676.
32. **Thiel, C., M. Osborn, and V. Gerke.** 1992. The tight association of the tyrosine kinase substrate annexin II with the submembranous cytoskeleton depends on intact p11- and Ca^{2+}-binding sites. J. Cell Sci. **103:**733–742.
33. **Thiery, J. P.** 2002. Epithelial-mesenchymal transitions in tumour progression. Nat. Rev. Cancer **2:**442–454.
34. **Vardouli, L., A. Moustakas, and C. Stournaras.** 2005. LIM-kinase 2 and cofilin phosphorylation mediate actin cytoskeleton reorganization induced by transforming growth factor-beta. J. Biol. Chem. **280:**11448–11457.
35. **Yamada, A., K. Irie, T. Hirota, T. Ooshio, A. Fukuhara, and Y. Takai.** 2005. Involvement of the annexin II-S100A10 complex in the formation of E-cadherin-based adherens junctions in Madin-Darby canine kidney cells. J. Biol. Chem. **280:**6016–6027.

36. **Zeisberg, M., and R. Kalluri.** 2004. The role of epithelial-to-mesenchymal transition in renal fibrosis. J. Mol. Med. **82:**175–181.
37. **Zhang, Z., G. Izaguirre, S. Y. Lin, H. Y. Lee, E. Schaefer, and B. Haimovich.** 2004. The phosphorylation of vinculin on tyrosine residues 100 and 1065, mediated by SRC kinases, affects cell spreading. Mol. Biol. Cell **15:**4234–4247.
38. **Zobiack, N., U. Rescher, S. Laarmann, S. Michgehl, M. A. Schmidt, and V. Gerke.** 2002. Cell-surface attachment of pedestal-forming enteropathogenic *E. coli* induces a clustering of raft components and a recruitment of annexin 2. J. Cell Sci. **115:**91–98.
39. **Zobiack, N., U. Rescher, C. Ludwig, D. Zeuschner, and V. Gerke.** 2003. The annexin 2/S100A10 complex controls the distribution of transferrin receptor-containing recycling endosomes. Mol. Biol. Cell **14:**4896–4908.